ELSEVIER

Electric Power Systems Research 62 (2002) 1–11

ELECTRIC POWER SYSTEMS RESEARCH

www.elsevier.com/locate/epsr

Development of models for analyzing the load-following performance of microturbines and fuel cells

Y. Zhu, K. Tomsovic *

School of EECS, Washington State University, Pullman, WA 99164-2752, USA

Received 4 September 2001; received in revised form 7 December 2001; accepted 7 December 2001

Abstract

Utility restructuring, technology evolution, public environmental policy, and expanding power demand are providing the opportunity for microturbines and fuel cells to become important energy resources. Deregulation has begun to allow for the provision of various ancillary services, such as load-following. In order to investigate the ancillary services ability of these units in distribution systems, new simulation tools are needed. This paper presents simplified slow dynamic models for microturbines and fuel cells. Their stand-alone dynamic performances are analyzed and evaluated. A distribution system embedded with a microturbine plant and an integrated fuel cell power plant is used as an example. The control strategy and load-following service in this distribution system are simulated. It is illustrated that microturbines and fuel cells are capable of providing load-following service, significantly enhancing their economic value.

Keywords: Microturbine; Fuel cell; Dynamic model; Load-following; Distribution system; Dynamic simulation; Ancillary service

1. Introduction

Today, with electric utility restructuring, public environmental policy, and expanding power demand, small distributed generators are in great need in order to satisfy on-site customer energy needs. Major improvements in the economic, operational, and environmental performance of small, modular units have been achieved through decades of intensive research. Among such distributed energy resources (DERs), microturbines and fuel cells show particular promise as they can operate on multiple fuels with low emissions, high efficiency and high reliability.

Microturbines are small and simple-cycle gas turbines with outputs ranging from around 25 to 300 kW. They are one part of a general evolution in gas turbine technology. Techniques incorporated into the larger machines to improve performance can be typically found in microturbines as well. These include recuperation, low NO_X technologies, and the potential use of advanced materials such as ceramics for hot section parts [1]. There are essentially two types of microturbines. One is a high-speed single-shaft unit with the compressor and turbine mounted on the same shaft as the electrical alternator. Turbine speeds mainly range from 50 000 to 120 000 rpm. The other type of microturbines is a split-shaft design that uses a power turbine rotating at 3600 rpm and a conventional generator connected via a gearbox.

Fuel cells are another rapidly developing generation technology. Fuel cells feature the potential for high efficiency (35–60%), low to zero emissions, quiet operation, and high reliability due to the limited number of moving parts. They produce power electrochemically by passing a hydrogen-rich gas over an anode and air over a cathode, and introducing an electrolyte in between to enable exchange of ions. The effectiveness of this process is strongly dependent upon the electrolyte to create the chemical reactivity needed for ion trans-

* Corresponding author. Tel.: +1-509-335-8260; fax: +1-509-335-3818.

E-mail address: tomsovic@eecs.wsu.edu (K. Tomsovic).

0378-7796/02/$ - see front matter
PII: S0378-7796(02)00033-0

port. As a result, fuel cells are classified by the electrolyte type:

- Polymer electrolyte fuel cell (PEFC)
- Alkaline fuel cell (AFC)
- Phosphoric acid fuel cell (PAFC)
- Molten carbonate fuel cell (MCFC)
- Solid oxide fuel cell (SOFC)

According to Ref. [2], today, PAFCs have been successfully commercialized. The 200 kW PAFC on-site plant, the PC-25, was one of the first to enter the commercial market. Second generation fuel cells, which are SOFCs and MCFCs, are expected to enter the market in 2002. PEFCs are still in the development and testing phase.

As microturbines and fuel cells will likely become major DERs in the future, dynamic models are necessary to deal with issues in system planning, operation and management. In particular, little of the development has been placed on effective operations. More specifically, an important operation issue is the provision of interconnected operations service (IOS), or ancillary services, under deregulation. According to the base case study [3], 'ancillary service costs amount to about 10% of the direct energy costs that customers experience', and of this, 20% for load-following and 15% for regulation. That is, load-following and regulation, which are substantially the same service except for the time frame, together account for 35% of the total IOS costs. Furthermore for the power loss ancillary service, while outside the scope of this study, proper placement and dispatch can have as much as a 10% impact on the effective capacity of a unit [4]. Assuming that proper economic methods are employed in the development of ancillary service markets, these services can provide a significant percentage of the value of a DER unit.

Microturbines and fuel cells have several unique properties from a modeling viewpoint. Microturbines have extremely low inertia and damping. In fuel cells, the electrical response time of the power section is generally fast, being mainly associated with the speed at which the chemical reaction is capable of restoring the charge that has been drained by the load. Conversely, the chemical response time of the reformer is usually slow, being associated with the time for the fuel cell stack to modify the chemical reaction parameters after a change in the flow of reactants. Accordingly, it is necessary to develop new models appropriate for investigating such performance.

The organization of this paper is as follows. The microturbine model is given in the next section, followed by the integrated fuel cell system model in 3. In 4, a test distribution system with a microturbine plant and a fuel cell plant is developed. The load-following capability of the units is demonstrated. Conclusions are given in 5. All variable definitions are provided at the end of the paper.

2. Microturbine modeling

As previously mentioned, there are essentially two types of microturbine designs. One is a high-speed single-shaft design with the compressor and turbine mounted on the same shaft as the alternator. Another is a split-shaft design that uses a power turbine rotating at 3600 rpm and a conventional generator (usually induction generator) connected via a gearbox. The designs are composed of the following four or five parts:

- *Turbine*. There are two kinds of turbines, high-speed single-shaft turbines and split-shaft turbines. All are small gas turbines.
- *Alternator or conventional machine*. In the single-shaft design, an alternator is directly coupled to the single-shaft turbine. The rotor is either a two- or four-pole permanent magnet design, and the stator is a conventional copper wound design. In the split-shaft design, a conventional induction or synchronous machine is mounted on the power turbine via a gearbox.
- *Power electronics*. In the single-shaft design, the alternator generates a very high frequency three-phase signal ranging from 1500 to 4000 Hz. The high frequency voltage is first rectified and then inverted to a normal 50 or 60 Hz voltage. In the split-shaft turbine design, power inverters are not needed.
- *Recuperator*. The recuperator is a heat exchanger, which transfers heat from the exhaust gas to the discharge air before it enters the combustor. This reduces the amount of fuel required to raise the discharge air temperature to that required by the turbine.
- *Control and communication systems*. Control and communication systems include full control of the turbine, power inverter and start-up electronics as well as instrumentation, signal conditioning, data logging, diagnostics, and user control communication.

Here, we are mainly interested in the slow dynamic performance. Based on this, our simplified microturbine model is founded on the following assumptions:

- System operation is under normal operating conditions. Start-up, shutdown, fast dynamics (faults, loss of power, etc.) are not included.
- The microturbine's electric-mechanical behavior is our main interest. The recuperator is not included in the model as it is only a heat exchanger to raise

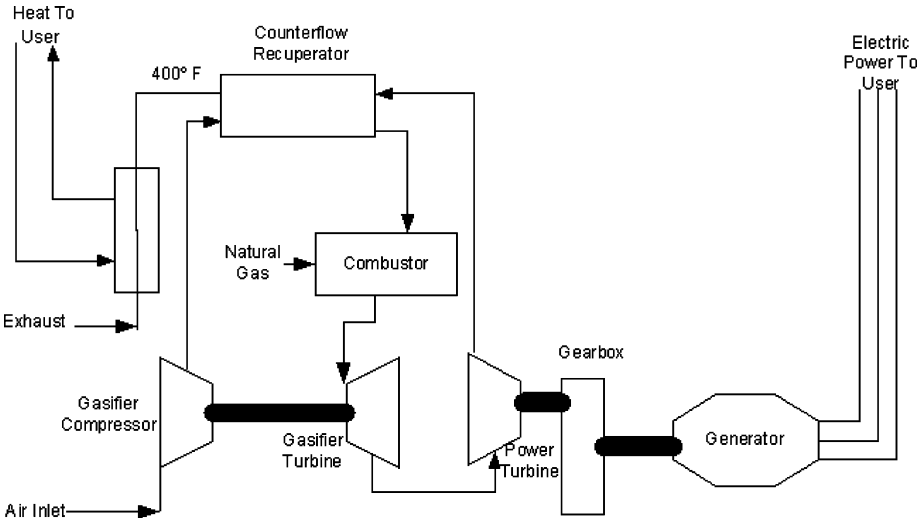

Fig. 1. PowerWorks microturbine diagram.

engine efficiency. Also, due to the recuperator's very slow response time, it has little influence on the time-scale of our dynamic simulations.

- The gas turbine's temperature control and acceleration control are of no significance under normal system conditions. They can be omitted in the turbine model.
- Most microturbines do not have governors and so a governor model is not considered.

2.1. Modeling of split-shaft design

Fig. 1 shows the diagram of a split-shaft design [1]. The main blocks in this microturbine model are shown in Fig. 2. The details of these blocks with all parameters are given in the following.

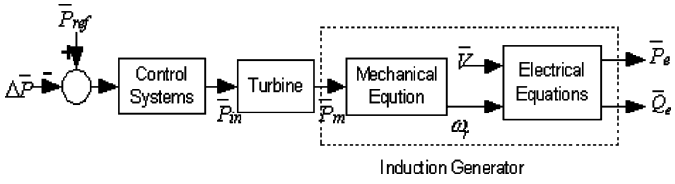

Fig. 2. Main blocks in microturbine model.

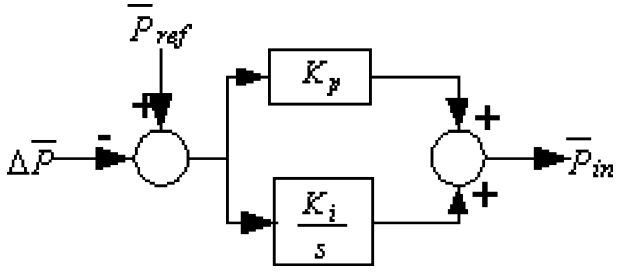

Fig. 3. Control system model.

2.1.1. Control systems

We are mainly interested in the real power control function of the control systems, so the control systems are simplified as a real power proportional-integral (PI) control function as in Fig. 3. The controlled real power $\bar{P}_{in}$ is applied to the turbine.

2.1.2. Turbine

In the split-shaft design, although there are two turbines, one is a gasifier turbine driving a compressor and another is a free power turbine driving a generator at rotating speed of 3600 rpm, there is only one combustor and one gasifier compressor. This is largely different from the twin-shaft combustion-turbine, which has two combustors and two compressors [5]. So it is more suitable to model this split-shaft turbine as a simple-cycle, single-shaft gas turbine. The GAST turbine-governor model is one of the most commonly used dynamic model of gas turbine units. The model is simple and follows typical modeling guidelines [6]. For simplicity and wider acceptability, the turbine part in this microturbine design is modeled as GAST model without the droop as in Fig. 4.

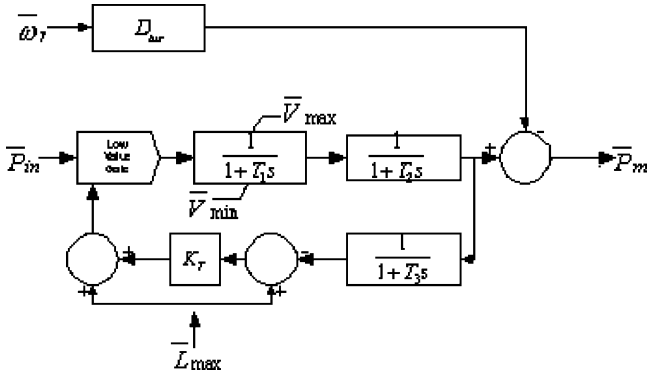

Fig. 4. Turbine model.

2.1.3. Mechanical equation

The mechanical equation of a generator is

$$2H\frac{\mathrm{d}\bar{\omega}_\mathrm{r}}{\mathrm{d}t}=\frac{\bar{P}_\mathrm{m}}{\bar{\omega}_\mathrm{m}}-\bar{P}_\mathrm{e}-D_\mathrm{gen}(\bar{\omega}_\mathrm{r}-1) \tag{1}$$

with $\bar{\omega}_\mathrm{r}=\bar{\omega}_\mathrm{m}$ and $\bar{\omega}_\mathrm{m}=\omega_\mathrm{m}/\omega_\mathrm{b}$, we have the following mechanical equation

$$2H\frac{\mathrm{d}\omega_\mathrm{m}}{\mathrm{d}t}=\frac{\omega_\mathrm{b}^2}{\omega_\mathrm{m}}\bar{P}_\mathrm{m}-\omega_\mathrm{b}\bar{P}_\mathrm{e}-D_\mathrm{gen}(\omega_\mathrm{m}-\omega_\mathrm{b}) \tag{2}$$

2.1.4. Electrical equations

2.1.4.1. Transformation from abc variables to dq0 variables. In the simulations here, the load flow solutions to the network equations will provide a pseudo-dynamic three-phase voltage $\bar{V}$ phasor in the abc reference frame. That is, the frequency is assumed to be constant throughout the distribution feeder and close to 60 Hz. This still allows for studies of disturbances and unbalanced conditions but not transient stability. The transformation between these representations is depicted as shown in Fig. 5.

The standard transformation between the synchronous rotating reference frame and abc variables is [7]

$$\begin{bmatrix}f_\mathrm{qs}\\ f_\mathrm{ds}\\ f_\mathrm{0s}\end{bmatrix}=\frac{2}{3}\begin{bmatrix}\cos\theta & \cos(\theta-2\pi/3) & \cos(\theta+2\pi/3)\\ \sin\theta & \sin(\theta-2\pi/3) & \sin(\theta+2\pi/3)\\ 1/2 & 1/2 & 1/2\end{bmatrix}\times\begin{bmatrix}f_\mathrm{as}\\ f_\mathrm{bs}\\ f_\mathrm{cs}\end{bmatrix} \tag{3}$$

and

$$\begin{bmatrix}f_\mathrm{qr}\\ f_\mathrm{dr}\\ f_\mathrm{0r}\end{bmatrix}=\frac{2}{3}\begin{bmatrix}\cos\beta & \cos(\beta-2\pi/3) & \cos(\beta+2\pi/3)\\ \sin\beta & \sin(\beta-2\pi/3) & \sin(\beta+2\pi/3)\\ 1/2 & 1/2 & 1/2\end{bmatrix}\times\begin{bmatrix}f_\mathrm{ar}\\ f_\mathrm{br}\\ f_\mathrm{cr}\end{bmatrix} \tag{4}$$

The inverse transformation from dq0 variables to abc variables can be easily derived from the above.

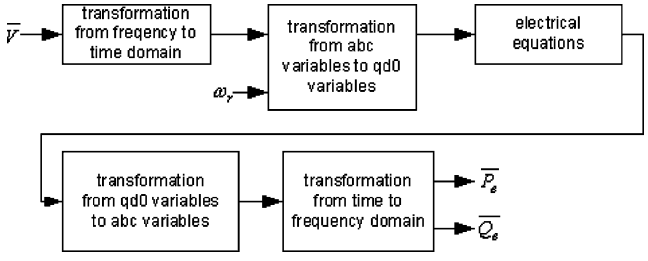

Fig. 5. Components in electrical equations model.

Table 1
Parameters in split-shaft microturbine model

Parameter	Representation	Value
P_rate	Rated power	250 kW
V_rate	Rated voltage	660 V
$\bar{P}_\mathrm{ref}$	Real power reference	1.0
K_p	Proportional gain in PI	1.0
K_i	Integral gain in PI	1.08
D_tur	Damping of turbine	0.03
T_1	Fuel system lag time constant 1	10.0 s
T_2	Fuel system lag time constant 2	0.1 s
T_3	Load limit time constant	3.0 s
$\bar{L}_\mathrm{max}$	Load limit	1.2
$\bar{V}_\mathrm{max}$	Maximum value position	1.2
$\bar{V}_\mathrm{min}$	Minimum value position	−0.1
K_T	Temperature control loop gain	1.0
H	Generator inertia	8.22 s
D_gen	Damping of generator	0.1
p	Number of poles	4
X_ls	Leakage reactance of stationary circuit	0.07620 Ω
X_lr	Leakage reactance of rotor circuit referred to the stator windings	0.23289 Ω
r_s	Resistance of stationary circuit	0.00708 Ω
r_r	Resistance of rotor circuit referred to the stator windings	0.00759 Ω
X_m	$X_\mathrm{m}=(3/2)X_\mathrm{ms}$, X_ms is magnetizing reactance of stationary circuit	3.44979 Ω

Assume this microturbine has 120% peak power capacity, so $\bar{L}_\mathrm{max}=\bar{V}_\mathrm{max}=1.2$.

2.1.4.2. Electrical equations for induction generator. Usually, induction generators are used in the split-shaft design. The electrical equations of the induction generator are most easily expressed in the dq0 reference frame. The electrical equations include flux linkage equation, stationary circuit electrical equation, and rotor circuit electrical equation. The flux linkage equation is

$$\begin{bmatrix}\lambda_\mathrm{ds}\\ \lambda_\mathrm{qs}\\ \lambda_\mathrm{dr}\\ \lambda_\mathrm{qr}\end{bmatrix}=\begin{bmatrix}L_\mathrm{ls}+M & 0 & M & 0\\ 0 & L_\mathrm{ls}+M & 0 & M\\ M & 0 & L_\mathrm{lr}+M & 0\\ 0 & M & 0 & L_\mathrm{lr}+M\end{bmatrix}\times\begin{bmatrix}i_\mathrm{ds}\\ i_\mathrm{qs}\\ i_\mathrm{dr}\\ i_\mathrm{qr}\end{bmatrix} \tag{5}$$

where $M=(3/2)L_\mathrm{ms}$. The stator circuit equation is

$$\begin{cases}\dfrac{\mathrm{d}}{\mathrm{d}t}\lambda_\mathrm{ds}=\omega_\mathrm{e}\lambda_\mathrm{qs}+v_\mathrm{ds}-r_\mathrm{s}i_\mathrm{ds}\\ \dfrac{\mathrm{d}}{\mathrm{d}t}\lambda_\mathrm{qs}=-\omega_\mathrm{e}\lambda_\mathrm{ds}+v_\mathrm{qs}-r_\mathrm{s}i_\mathrm{qs}\end{cases} \tag{6}$$

and the rotor circuit equation is

$$\begin{cases} \dfrac{\mathrm{d}}{\mathrm{d}t}\lambda_{\mathrm{dr}} = (\omega_{\mathrm{e}} - \omega_{\mathrm{r}})\lambda_{\mathrm{qr}} + v_{\mathrm{dr}} - r_{\mathrm{r}} i_{\mathrm{dr}} \\ \dfrac{\mathrm{d}}{\mathrm{d}t}\lambda_{\mathrm{qr}} = -(\omega_{\mathrm{e}} - \omega_{\mathrm{r}})\lambda_{\mathrm{dr}} + v_{\mathrm{qr}} - r_{\mathrm{r}} i_{\mathrm{qr}} \end{cases} \quad (7)$$

Most induction machines have squirrel-cage rotor where $v_{\mathrm{dr}} = 0$ and $v_{\mathrm{qr}} = 0$.

2.1.5. Model parameters

For the examples studied here, we assume the rated power of the microturbine is 250 kW, and the rated line voltage is 660 V. The parameters in this microturbine model are updated from Refs. [6,8] and listed in Table 1.

2.2. Modeling of a single-shaft design [9]

The single-shaft microturbine has electrical alternator, air compressor, and turbine mounted on a single rotating shaft. The shaft turns between 50k and 120k rpm, and the alternator generates a high frequency three-phase ac ranging from 1500 to 4000 Hz. This requires a power electronic interface, which consists of an ac to dc rectifier, a dc bus with a capacitor, and a dc to ac inverter. In Ref. [9], a very simplified single-shaft microturbine model is presented based on the following assumptions:

- There is adequate energy storage on the dc bus so that the microturbine can be seen as an ideal, no-load permanent magnet generator with constant dc potential.
- The ac to dc converters are full-wave rectifiers with constant current outputs.
- All losses are neglected.

Details of the model are in Ref. [9].

2.3. Evaluation of stand-alone performance

It is important to evaluate the appropriateness of the developed models for our system studies. Here, we make some observations based on the stand-alone dynamic performance of the split-shaft microturbine model. Assume a split-shaft microturbine system is operating with constant rated voltage 1.0 p.u. and power demand 0.7 p.u. All parameters are the same as in Table 1. At $t = 0.5$ s, there is a step increase of power demand from 0.7 to 1.0 p.u. Fig. 6 shows the dynamic response of mechanical power $\bar{P}_{\mathrm{m}}$ input and total three-phase electrical power output $\bar{P}_{\mathrm{e}}$ in this microturbine system.

From the simulation, note the following:

- The initial response time for the step change is around 10 s. This delay is mainly due to the turbine response time.

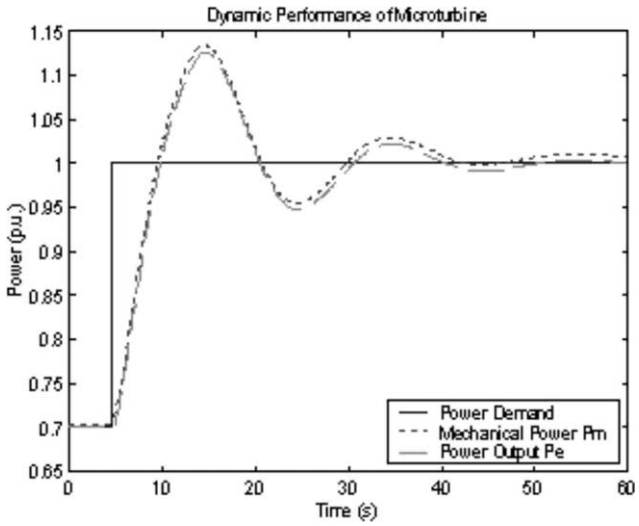

Fig. 6. Dynamic response of microturbine system.

- For the electrical power $\bar{P}_{\mathrm{e}}$ response, the oscillation is significant with a time period around 20 s. This is mainly due to the small inertia and damping in the microturbine.
- This microturbine model appears suitable for the time scale to be used in our dynamic simulation.

3. Integrated fuel cell system modeling

A power generation fuel cell system has the following three main parts:

- *Fuel processor*. The fuel processor converts fuels such as natural gas to hydrogen and byproduct gases.
- *Power section (fuel cells)*. The power section generates the electricity. There are numerous individual electrochemical fuel cells in the power section.
- *Power conditioner*. The power conditioner converts dc power to ac power output and includes current, voltage and frequency control.

Although the second generation fuel cells, such as MCFCs or SOFCs, are still in the development stage, they have great potential to achieve high efficiency and good performance and are near commercialization now [2]. As a result, we focus on SOFC system modeling with the expectation that the response time of other types of cells would be similar.

3.1. Modeling of SOFC system

Ref. [10] provides a basic SOFC power section dynamic model used for performance analysis during normal operation. Based on that, some control strategies of the fuel cell system, response functions of fuel

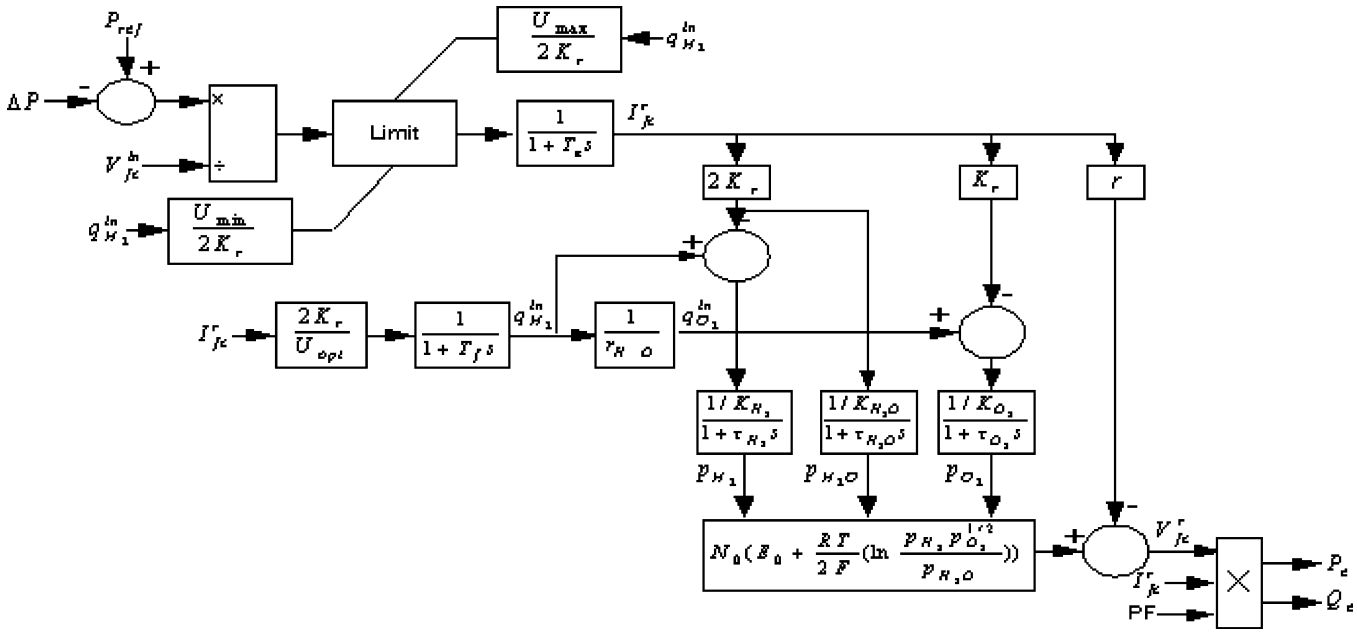

Fig. 7. SOFC system dynamic model.

processor and power section are added to model the SOFC power generation system.

(a) Although CO can be a fuel in SOFC, the CO-shift reaction is chemically favored with present designs and operations if the fuel gas contains water. The CO-shift reaction is:

$$CO + H_2O \rightarrow CO_2 + H_2 \tag{8}$$

Based on this, we assume that only H_2 and O_2 enter into the fuel cells.

(b) Fuel utilization is the ratio between the fuel flow that reacts and the input fuel flow. Here, we have,

$$U_f = q^r_{H_2}/q^{in}_{H_2} \tag{9}$$

Typically, an 80–90% fuel utilization is used. Ref. [10] gives the following equation:

$$q^r_{H_2} = \frac{N_0 I^r_{fc}}{2F} = 2K_r I^r_{fc} \tag{10}$$

For a certain input hydrogen flow, the demand current of the fuel cell system can be restricted in the range

$$\frac{0.8q^{in}_{H_2}}{2K_r} \leqslant I^{in}_{fc} \leqslant \frac{0.9q^{in}_{H_2}}{2K_r} \tag{11}$$

(c) The real output current in the fuel cell system can be measured, so the input fuel flow can be controlled to control U_f at 85%, so

$$q^{in}_{H_2} = \frac{2K_r I^r_{fc}}{0.85} \tag{12}$$

(d) The peak power capacity is the ratio of maximum theoretical power delivery to the rated power in the fuel cell system. It is only determined with the available active fuel cell area. For the highest possible total efficiency and the dynamic load-following behavior, p_k should be as large as possible. As this value is directly proportional to the effective fuel cell area for a constant output, cost considerations restrict the upper value with values between 130 and 180% preferred [11]. In practice, this upper value is also restricted by the safety of system operation. In order to prevent damage to the electrolyte, the fuel cell pressure difference between the hydrogen and oxygen passing through the anode and cathode gas compartments should be below 4 kPa under normal operation and 8 kPa under transient conditions [12]. Because different fuel cell systems have different peak power capacity, by simulation it is shown that p_k in our fuel cell system model should be below 170%, which means the maximum power delivery of our fuel cell system is below 1.7 times of the rated power.

(e) The overall fuel cell reaction is:

$$H_2 + \frac{1}{2}O_2 \rightarrow H_2O \tag{13}$$

So, the stoichiometric ratio of hydrogen to oxygen is 2 to 1. Oxygen excess is always taken in to let hydrogen react with oxygen more completely. Simulation in our fuel cell system shows that r_{H_O} should be kept around 1.145 in order to keep the fuel cell pressure difference below 4 kPa under normal operation. So the input oxygen flow is controlled to keep r_{H_O} at 1.145 by speed control of the air compressor.

(f) The chemical response in the fuel processor is usually slow as it is associated with the time to change the chemical reaction parameters after a change in the flow of reactants. This dynamic response function is

Table 2
Parameters in SOFC system model

Parameter	Representation	Value
P_{rate}	Rated power	100 kW
P_{ref}	Real power reference	100 kW
T	Absolute temperature	1273 K
F	Faraday's constant	96 487 C/mol
R	Universal gas constant	8314 J/(kmol K)
E_0	Ideal standard potential	1.18 V
N_0	Number of cells in series in the stack	384
K_r	Constant, $K_r = N_0/4F$	0.996×10^{-6} kmol/(s A)
U_{max}	Maximum fuel utilization	0.9
U_{min}	Minimum fuel utilization	0.8
U_{opt}	Optimal fuel utilization	0.85
K_{H_2}	Valve molar constant for hydrogen	8.43×10^{-4} kmol/(s atm)
K_{H_2O}	Valve molar constant for water	2.81×10^{-4} kmol/(s atm)
K_{O_2}	Valve molar constant for oxygen	2.52×10^{-3} kmol/(s atm)
τ_{H_2}	Response time for hydrogen flow	26.1 s
τ_{H_2O}	Response time for water flow	78.3 s
τ_{O_2}	Response time for oxygen flow	2.91 s
r	Ohmic loss	0.126 Ω
T_e	Electrical response time	0.8 s
T_f	Fuel processor response time	5 s
r_{H_O}	Ratio of hydrogen to oxygen	1.145
PF	Power factor	1.0

For tubular SOFC, the optimal operating temperature is around 1273 K. The ideal standard potential E_0 of an H_2/O_2 fuel cell is 1.229 V with liquid water product and 1.18 V with gaseous water product (at 1 atm and 198 K) [2]. For SOFC, $E_0 = 1.18$ V. The rated voltage $V_{rate} = 333.8$ V under rated power output. The ideal equilibrium potential E can be calculated as $N_0E - r(P_{rate}/V_{rate}) = V_{rate}$ so $E = 0.97$ V. This corresponds to the results in Fig. 2-1 of Ref. [2]. The average oxygen partial pressure in the cathode flow is within the range of 0.16–0.20 bar [13]. In this model, the average partial pressures of oxygen and hydrogen are both around 0.18 bar at rated power output. Assume the PF is kept constant as 1.0.

modeled as a first-order transfer function with a 5-s time constant.

(g) The electrical response time in the fuel cells is generally fast and mainly associated with the speed at which the chemical reaction is capable of restoring the charge that has been drained by the load. This dynamic response function is also modeled as a first-order transfer function but with a 0.8-s time constant.

(h) Through the power conditioner, the fuel cell system can output not only real power but also reactive power. Usually, PF can be in the range of 0.8–1.0. Because the response time of the power conditioner is less than 10 ms, it is not necessary to include its detailed model in our slow dynamic fuel cell system except we can assume that PF can be adjusted accordingly by the power conditioner.

Based on Ref. [10] and the above discussions, the SOFC system dynamic model is given in Fig. 7, where $q^{in}_{O_2}$ is oxygen input flow.

3.1.1. Model parameters

We assume the rated power of this SOFC system is 100 kW. The model parameters are updated from Ref. [10] and listed in Table 2.

3.2. Evaluation of stand-alone performance

Assume a stand-alone SOFC fuel cell system is operating with constant rated voltage 1.0 p.u. and power demand 0.7 p.u. All parameters are the same as Table 2. At $t = 5$ s, there is a step increase of power demand from 0.7 to 1.0 p.u. Fig. 8 shows the dynamic response of this system.

From simulation, note the following:

- In the first 2 or 3 s after $\bar{P}_D$ is increased, $\bar{P}_e$ has a rapid increase due to the fast electrical response time in the fuel cells. Subsequently, $\bar{P}_e$ increases slowly and continuously until reaching the required power. This is due to the slow chemical response time in the fuel processor. The total response time of $\bar{P}_e$ from 0.7 to 0.98 p.u. is about 30 s. This is roughly three times that of the microturbine's response time.
- The fuel cell pressure difference between hydrogen and oxygen increases to the peak value of 3.5 kPa, which is less than the maximum safety pressure difference 8 kPa. It then returns to the normal operating pressure difference value around 0 kPa.
- Due to the power demand increase, the fuel utilization increases to the maximum fuel utilization in about 5 s. After staying at U_{max} for 25 s, it decreases to U_{opt} in about 20 s.
- This SOFC system model appears suitable for the time scale to be used in our dynamic simulation.

4. Simulation of load-following performance

Dynamic simulations of load-following service provided by a microturbine plant G11 and a fuel cell plant G2 are performed on the system in Fig. 9, which is based on a distribution feeder in the Kumamoto area of Japan. The network parameters can be found in Ref. [14], where the base power is 10 MV A and the base line voltage is 6.6 kV. G2 is connected at bus 2, which consists of seven 3-phase SOFC stacks. Each 3-phase stack is the same, having three single-phase fuel cell systems with $P_{rate} = 100$ kW and $V_{rate} = 333.8$ V, which can be modeled as in Fig. 7, yielding a rated power of 2.1 MW. G11 is connected at bus 11 and consists of ten microturbines. Each microturbine has the same parameters, which can be represented as our 250 kW, 660 V split-shaft model, yielding a rated power of 2.5 MW. Suppose at a certain time, the total load in this distribution system is $P_{load} = 18.9$ MW, $Q_{load} = 1.3$ Mvar. The units at G2 and G11 mainly provide some

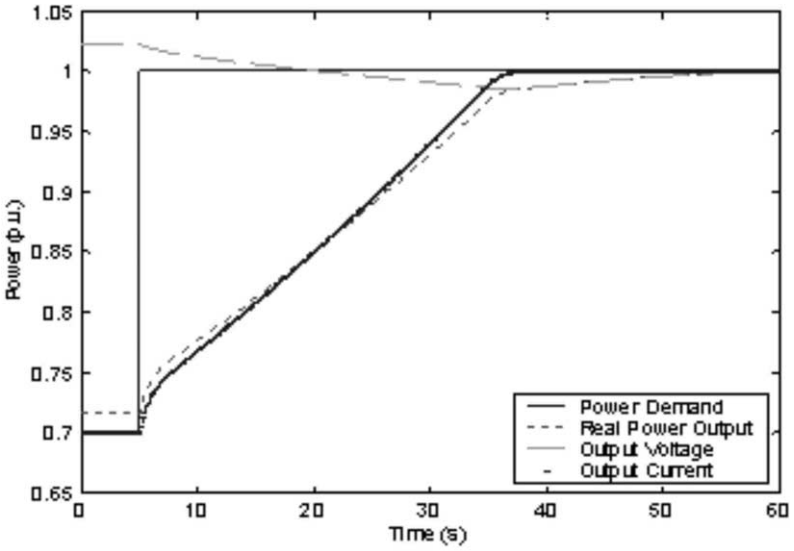

(a) response of $\overline{P}_D, \overline{P}_e, \overline{V}^r_{fc}, \overline{I}^r_{fc}$

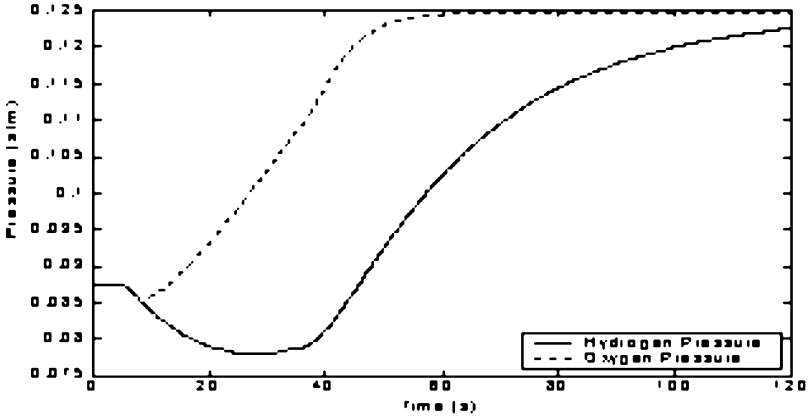

(b) response of p_{H_2}, p_{O_2}

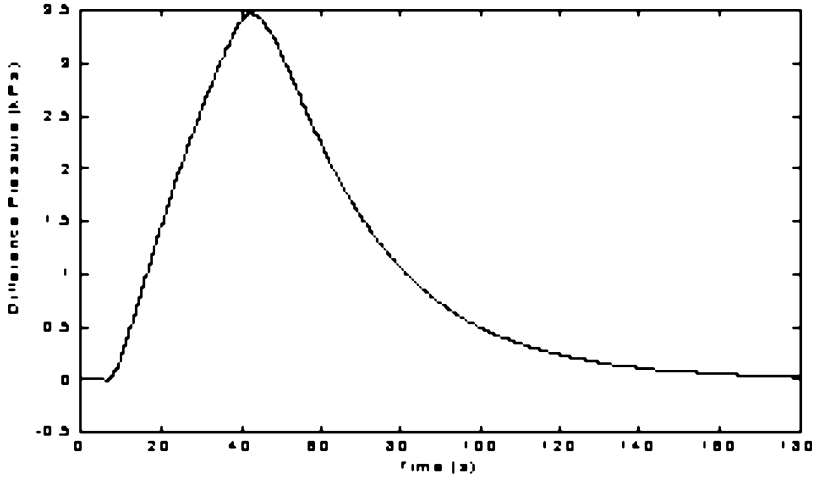

(c) response of pressure difference between hydrogen and oxygen

Fig. 8. Dynamic response of SOFC system. (a) response of $\bar{P}_{\mathrm{D}}$, $\bar{P}_{\mathrm{e}}$, $\bar{V}^{\mathrm{r}}_{\mathrm{fc}}$, $\bar{I}^{\mathrm{r}}_{\mathrm{fc}}$; (b) response of P_{H_2}, P_{O_2}; (c) response of pressure difference between hydrogen and oxygen; (d) response of fuel utilization.

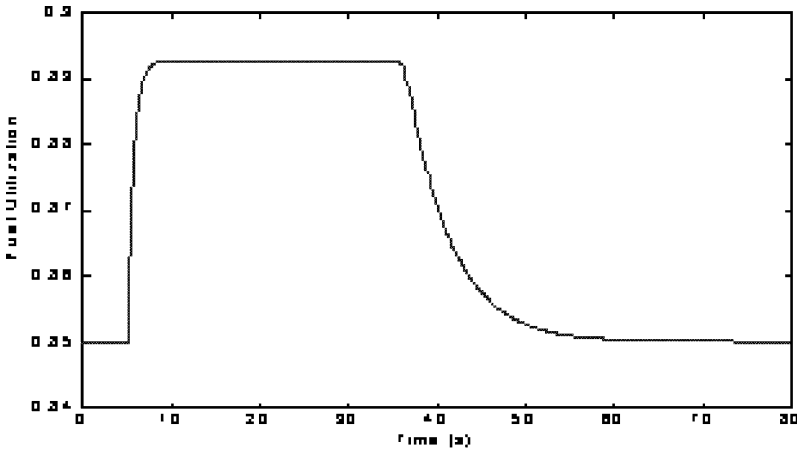

(d) response of fuel utilization

Fig. 8 (*Continued*)

peak shaving capability and ancillary services for the feeder.

Based on the importance of load-following service, the focus is on dynamic simulation of load-following performance of the plants G2 and G11. The following assumptions are made in this simulation:

- The traditional load-following and regulation functions used frequency deviation and tie-line mismatches to adjust generator set points. Because the feeder load is small relative to overall system, the frequency deviation is best ignored in performing the load-following function. We refer to the power delivered from the transmission system into the feeder as the 'tie-line' flow and it is set at $P_{set} =$ 0.16 MW in these studies.
- In using only the 'tie-line' flow, we assume bilateral contracts to perform load-following among DERs at a given feeder is not allowed. That is, the ancillary service must be coordinated at the substation or transmission level.
- There is a very simple communication system in this distribution system. The feeder can measure the 'tie-line' flow and then broadcasts it to all DERs. For simplicity, all DERs receive the signal with some delay, which is modeled here 0.5 s.
- Because the efficiency of fuel cell plant is about 60%, much higher than the 30% efficiency of the microturbine plant, G2 produces as much power as possible. At the same time, each power output must stay within static and transient ratings. During load-following, G2 and G11 work together to pick up the load variance in order to keep the 'tie-line' flow constant. As G2's output reaches its rated maximum, G11 will pick up the deficiency.
- It is desirable to minimize the number of dynamic equations to be solved in the simulations. Here, all microturbines in the plant G11 are regarded as coherent machines, which have the same dynamic response and share the generation equally. Similarly, the fuel cell stacks at G2 respond in concert.

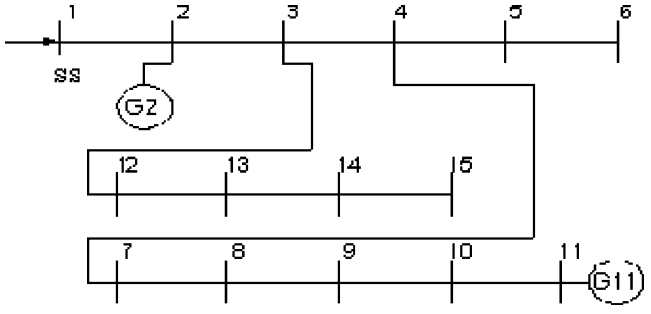

Fig. 9. Kumamoto 15-bus distribution system diagram.

Assume there is a 5% of step increase in the total load at $t = 5$ s, Fig. 10 shows the dynamic response of 'tie-line' flow, real power output of G2, and real power

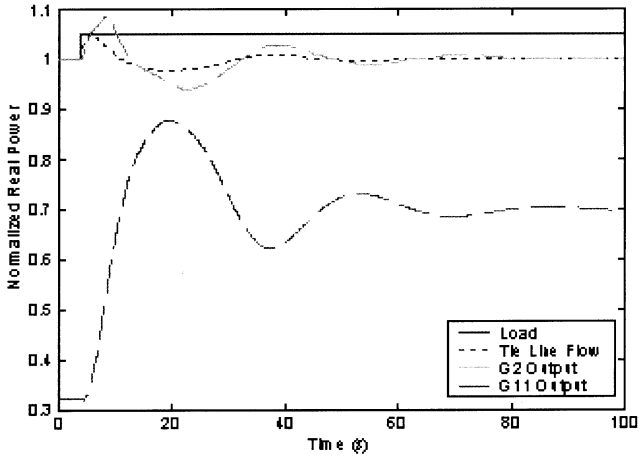

Fig. 10. Load-following performance of microturbines and fuel cells.

output of G11. From the simulation, observe the following:

- Originally, the fuel cells plant G2 operates at rated power. During load fluctuations, the load-following service is mainly provided by the microturbine plant G11. After oscillations for about 100 s, G2 returns to its original rated power output, and the 'tie-line' flow is back to the original set point.
- The microturbine plant reaches the peak output in less than 15 s. This picks up the major increase in the load. The remaining needed increase and settling time requires around 100 s. Because the total load increase is 5% of the base load, 945 kW, the system load-following ability is about 10 kW/s.
- The microturbine and fuel cells are capable of providing effective load-following service in the distribution system.

5. Conclusions

In this paper, a simplified slow dynamic model of a split-shaft microturbines is developed. In addition, an integrated SOFC system model is expanded by defining appropriate control systems and parameters for the time frame of interest. Evaluations of these stand-alone models show that they are reasonable and suitable for slow dynamic simulations. A distribution system with some simple but practical control strategies is developed for the analysis of load-following service provided by microturbines and fuel cell systems. It is demonstrated that microturbines and fuel cells are capable of providing load-following service in the distribution system.

6. List of symbols

6.1. Microturbine variables

P_m	mechanical power
P	number of poles
ω_m	mechanical rotor speed
ω_r	electrical rotor speed
ω_e	synchronous electrical rotor speed, 377 rad/s for 60 Hz system
ω_b	synchronous mechanical rotor speed, $\omega_b = 2\omega_e/p$
f_{as}, f_{bs}, f_{cs}	abc variables of stator circuit
f_{ds}, f_{qs}, f_{os}	dq0 variables of stator circuit
f_{ar}, f_{br}, f_{cr}	abc variables of rotor circuit referred to the stator windings
f_{dr}, f_{qr}, f_{or}	dq0 variables of rotor circuit referred to the stator windings
θ	electrical angle by which q-axis leads the magnetic axis of stator phase-a winding
β	electrical angle by which q-axis leads the magnetic axis of rotor phase-a winding
λ	flux linkage
I	current
v	voltage
L_{ls}, L_{ms}	leakage or magnetizing inductance of stator circuit, respectively
L_{lr}, L_{mr}	leakage or magnetizing inductance of rotor circuit referred to the stator windings, respectively

6.2. Fuel cell variables

$q_{H_2}^{in}$, $q_{H_2}^{r}$	hydrogen flow of input or reacting respectively, kmol/s
P_{H_2}, P_{O_2}, P_{H_2O}	partial pressure of hydrogen, oxygen, or water respectively, atm
I_{fc}^{in}, I_{fc}^{r}	fuel cell system demand current or real output current respectively
V_{fc}^{in}, V_{fc}^{r}	fuel cell system input voltage or real output voltage respectively
U_f	fuel utilization
p_k	peak power capacity

6.3. Other variables

S_{base}	base power of the distribution system.
P_e	electrical real power
Q_e	electrical reactive power
ΔP	difference between power generated P_{gen} and power demand P_D, $\Delta P = P_{gen} - P_D$
V	three-phase voltage
I	three-phase current
V_a, V_b, V_c	abc voltage phasors
I_a, I_b, I_c	abc current phasors

Note: Overscores indicate the variable is given in per unit.

Acknowledgements

The authors would like to thank Prof. T. Hiyama for helpful discussions. This work was supported in part through Power Systems Engineering Research Center (PSerc) and the US Department of Energy.

References

[1] J.H. Watts, Microturbines: a new class of gas turbine engines, Gas Turbine News in Brief 39 (1) (1999) 5–11, http://www.asme.org/igti/ggtn/archives.html.
[2] EG & G Services, Parsons, Inc. and Science Applications International Corporation, Fuel Cell Handbook, fifth ed., Oct. 2000.
[3] E. Hirst, B. Kirby, Creating competitive markets for ancillary services, in: ORNL/CON-448, Oak Ridge National Laboratory, Oak Ridge, TN 1997.
[4] T. Griffin, K. Tomsovic, D. Secrest, et al., Placement of dispersed generations systems for reduced losses, Proceedings of the 33rd Hawaii International Conference on Systems Sciences, Maui, Hawaii, January 2000.
[5] L.N. Hannett, G. Jee, B. Fardanesh, A governor/turbine model for a twin-shaft combustion turbine, IEEE Trans. Power Syst. 10 (1) (1995) 133–140.
[6] M. Nagpal, A. Moshref, G.K. Morison, et al., Experience with testing and modeling of gas turbines, Proceedings of the IEEE/PES 2001 Winter Meeting, Columbus, Ohio, USA, January/February 2001, pp. 652–656.
[7] P.C. Krause, O. Wasynczuk, S.D. Sudhoff, Analysis of Electric Machinery (Chapter 4), IEEE Press, NJ 1995.
[8] A. Feijoo, J. Cidras, Analysis of mechanical power fluctuations in asynchronous WEC's, IEEE Trans. Energy Conv. 14 (3) (1999) 284–291.
[9] R.H. Lasseter, Control of distributed resources, Proceedings of the 1998 International Conference on Bulk Power Systems Dynamics and Control IV—Restructuring, Santorini, Greece, August 1998, pp. 323–330.
[10] J. Padulles, G.W. Ault, J.R. McDonald, An integrated SOFC plant dynamic model for power systems simulation, J. Power Sources 86 (2000) 495–500.
[11] B. Thorstensen, A parametric study of fuel cell system efficiency under full and part load operation, J. Power Sources 92 (2001) 9–16.
[12] W. He, Dynamic model for molten carbonate fuel-cell power-generation systems, J. Energy Conv. Manage. 39 (8) (1998) 775–783.
[13] S. Campanari, Thermodynamic model and parametric analysis of a tubular SOFC module, J. Power Sources 92 (2001) 26–34.
[14] S. Li, K. Tomsovic, T. Hiyama, Load following functions using distributed energy resources, Proceedings of the IEEE/PES 2000 Summer Meeting, Seattle, Washington, USA, July 2000, pp. 1756–1761.

Biographies

Y. Zhu received the B.S. from Tsinghua University, China, in 1989, and the M.S. from the Graduate School of Nanjing Automation Research Institute, China, in 1992, all in Electrical Engineering. He worked for NARI, China as a R&D engineer during 1992–1998. Currently, he is a graduate student at Washington State University. His current research interests include dynamic analysis and control of distributed generation.

K. Tomsovic received the B.S. from Michigan Technological University, Houghton, in 1982, and the M.S. and PhD degree from University of Washington, Seattle, in 1984 and 1987, respectively, all in Electrical Engineering. Currently, he is an Associate professor at Washington State University. From 1999 to 2000, he held the Kyushu Electric Chair for Advanced Technology at Kumamoto University in Japan. His research interests include Intelligent Systems and optimization methodologies applied to power systems problems.